Tuning Eu^{3+} emission in europium sesquioxide films by changing the crystalline phase

A. Mariscal[1], A. Quesada[2], I. Camps[1], F. J. Palomares[3], J. F. Fernández[2], R. Serna[1].

[1] Laser Processing Group, Instituto de Óptica, CSIC, C/Serrano 121, 28006 Madrid, Spain.
[2] Ceramics for Smart Systems Group, Instituto de Cerámica y Vidrio, C/ Kelsen 5, 28049 Madrid, Spain.
[3] Instituto de Ciencia de Materiales de Madrid, C/Sor Juana Inés de la Cruz 3, 28049 Madrid, Spain.

Abstract

We report the growth of europium sesquioxide (Eu_2O_3) thin films by pulsed laser deposition (PLD) in vacuum at room temperature from a pure Eu_2O_3 ceramic bulk target. The films were deposited in different configurations formed by adding capping and/or buffer layers of amorphous aluminum oxide (a-Al_2O_3). The optical properties, refractive index and extinction coefficient of the as deposited Eu_2O_3 layers were obtained. X-ray photoelectron spectroscopy (XPS) measurements were done to assess its chemical composition. Post-deposition annealing was performed at 500°C and 850 °C in air in order to achieve the formation of crystalline films and to accomplish photoluminescence emission. According to the analysis of X-ray diffraction (XRD) spectra, cubic and monoclinic phases were formed. It is found that the relative amount of the phases is related to the different film configurations, showing that the control over the crystallization phase can be realized by adequately designing the structures. All the films showed photoluminescence emission peaks (under excitation at 355 nm) that are attributed to the intra 4f-transitions of Eu^{3+} ions. The emission spectral shape depends on the crystalline phase of the Eu_2O_3 layer. Specifically, changes in the hypersensitive $^5D_0 \rightarrow {}^7F_2$ emission confirm the strong influence of the crystal field effect on the Eu^{3+} energy levels.

Keywords: Pulsed laser deposition, Europium, crystalline films, cubic phase, monoclinic phase, Al_2O_3 capping layer, photoluminescence, refractive index, crystal field, XRD, XPS.

1. Introduction

Europium oxide films have received large attention for their use in the fields of microelectronics, spintronics, lighting, magnetism and photonics, among others. However, applications remain a challenge due to the difficulties for the fabrication of high quality crystalline pure europium oxide thin films. Europium oxide (EuO_x) films growth on Si substrates has been usually obtained by two methods. In the first one, deposition is performed starting from a pure metallic europium target and the formation of the oxide is achieved by adding an oxygen gas partial pressure during deposition in order to obtain different stoichiometries [1]. In the second method, the authors start from a europium oxide target and use post-deposition annealing treatments in reduction atmospheres at high temperatures (1000 °C). However, in the second case, as a result of the high temperature post-annealing treatments and due to the direct deposition of the Eu oxide on the Si substrates, formation of Eu-silicate phases has been reported, which precludes obtaining pure europium oxide films [2–4].

The aim of this work is to report a simplified two step growth process, which yields stoichiometric, good quality, crystalline and optically active europium sesquioxide (Eu_2O_3) thin films with intense Eu^{3+} red light emission. We have prepared the thin films using pulsed laser deposition (PLD), which has proven to be excellent for the preparation of complex oxides, and production of high-density films with good adhesion [5]. To obtain good quality crystalline films, we used relatively low temperature annealing treatments in air. In fact, it will be shown that good crystallinity of both the cubic and monoclinic phases can be accomplished for temperatures as low as 500 °C.

2. Experimental

The PLD system consists of a UV laser ArF excimer (λ = 193 nm, 20 ns pulse duration) and a vacuum chamber equipped with a multi-target system that can accommodate up to four targets. In order to ablate the materials the laser beam was focused at an incidence angle of 45° onto the targets. During the process of ablation, the targets were rotated to prevent crater formation. The films were deposited on Silicon (100) wafers placed at 43 mm from the target surface at room temperature. The ablation was performed in the so called off-axis configuration, i.e. the centre of the substrate did not coincide exactly with the plasma expansion axis. The substrate was also rotated during deposition with the purpose to obtain a large area of homogeneous film thickness. All the experiments were performed at vacuum $1.3x10^{-6}$ mbar. The energy density value used to ablate the targets was chosen to be 3.5 J/cm^2. To calibrate film deposition rates, reference films of both materials, Eu_2O_3 and Al_2O_3 were grown separately. To monitor the growth progress, *in-situ* reflectivity measurements during growth of these reference films were performed with a chopped diode laser (647 nm), having an incidence angle of about 45° respect to the normal of the substrate surface.

For sample preparation two targets were used: a non-commercial Eu_2O_3 monoclinic phase target (fabricated by Ceramics of Smart Systems Group - CSIC), sintered at 1400°C for 2 h [6] and a commercial α-Al_2O_3 (99.9%) target. Films were prepared under three configurations by ablating alternatively the two targets: (a) Eu00: only the Eu_2O_3 optically active film was deposited in direct contact to the substrate (no capping nor buffer layers); (b) Eu11: the Eu_2O_3 film with buffer and capping layers, i.e., it was sandwiched between an a-Al_2O_3 buffer layer deposited on top of the substrate before the Eu_2O_3 film deposit, and a Al_2O_3 capping layer deposited on top of the film; finally (c) Eu01: only capping layer deposited on top of the Eu_2O_3 film. A scheme of the different thin film configurations is shown in Figure 1. In all films, the europium oxide layer (Eu_2O_3) and each of the a-Al_2O_3 buffer and capping layers, were set to have a thickness of 200 ± 10 nm and 25 ± 5 nm respectively. The role of the amorphous aluminum oxide (a-Al_2O_3) layers is twofold. First, they prevent the europium oxide layer from chemical reactions, either from the external environment (capping layer on top of the active film) or with the Si substrate (buffer layer on top of the Si substrate deposited) before the Eu_2O_3 film. Second, as it will be shown, the deposition of these layers influences the Eu_2O_3 crystallization. The a-Al_2O_3 is also a dense oxide that shows no crystalline structure up to 900 °C, is chemically stable at low temperatures and optically transparent, being suitable for luminescence applications [7,8].

After the films deposition, spectroscopic ellipsometry (SE) measurements were performed in the 300 nm to 1500 nm wavelength range at incidence angles of 60°, 65° and 70° using a VASE ellipsometer (J.A. Woollam Co., Inc.). The combined analyses of the optical in-situ and ex-situ measurements were used firstly, to obtain the film thickness of the reference films and secondly, to determine the deposition rates and optical linear properties for the as-grown films.

Post-deposition annealing treatments were performed in a furnace in air. The temperature was increased at rate of 10° C/min and the final temperature was maintained during one hour. The films were annealed at 300° C to activate emission, and then at 500° C, 700° C and 850° C. The photoluminescence was measured after each annealing treatment. The formation of the crystalline phases was assessed by using X-ray diffraction (XRD) (D8 Advance, Bruker, Germany) with Cu K_{α} radiation.

X-ray photoelectron spectroscopy (XPS) was used to characterize the chemical composition and the oxidation state of the samples. XPS spectra were acquired in an ultrahigh vacuum (UHV) chamber with a base pressure of 10^{-9} mbar equipped with a hemispherical electron energy analyzer (SPECS Phoibos 150 spectrometer) and a delay-line detector in the nine-segment mode, using a non-monochromatic AlKα (1486.61 eV) X-ray source. XPS spectra were recorded at normal emission take-off angle, using an energy step of 0.1 eV and a pass-energy of 20 eV [9,10]. A small amount of contaminants, carbon and hydroxyl (OH) species was detected in the sample surface because the samples were exposed to air after growth and prior to XPS measurements. The signal from adventitious carbon at 284.6 eV was used for energy calibration. This surface contamination was removed by Ar ion bombardment. The overall surface composition of as-grown samples was determined from survey spectra with regions of interest (Eu3d, O1s and C1s). The integral peak areas after background subtraction and normalization using sensitivity factors provided by electron energy analyzer manufacturer were used to calculate the atomic concentration of each element. Data processing was performed using CasaXPS software (Casa Software Ltd., Cheshire, UK).

Photoluminescence (PL) measurements were done under excitation at λ = 355 nm at a nominal power of 160 mW from a solid state Genesis CX 355-200 Optically Pumped Semiconductor Laser (Coherent). The light emitted by the sample was collected by a microscope objective (10X Mitutoyo Plan Apo NIR Infinity-Corrected Objective), focalized over a Czerny-Turner type Monochromator (Acton Spectra Pro 300i, with a diffraction grating of 1200 g/mm) and detected through a photomultiplier EMI 9659QB. The signal was amplified with the standard lock-in technique and collected by a CPU.

3. Results and discussion

i) Linear Optical Properties.

The complex refractive index (**n**=n+ik) of the active Eu_2O_3 films was determined from the spectroscopic ellipsometry (SE) measurements for the films in the different configurations. For the as-grown films, Figure 2 shows the corresponding refractive index (n) and extinction coefficient (k) values as a function of wavelength. The SE parameters of the Eu_2O_3 layers were fitted using a

Cauchy dispersion law for the refractive index, n (λ) = A + B/$λ^2$ + C/$λ^4$, with A, B, and C being free parameters. For the k value, the Urbach dispersion was used:

$$k(\lambda) = A_k \exp B_k\left(\frac{hc}{\lambda} - E_u\right) \quad (1)$$

where E_u is the Urbach energy [eV], and A_k and B_k are free parameters. For the refractive index of the Al_2O_3 layers (buffer and capping) data from [11] were used. The fit process was performed in three steps: 1) Eu00 was used to obtain the thickness and optical constants for the Eu_2O_3. 2) With these data fixed, the thickness for Al_2O_3 layer in Eu01 was fitted. 3) All the films were refitted with data feedback. The results yielded a thickness value for the Eu_2O_3 layer of 200 ± 10 nm for all the studied configurations and of 25 ± 5 nm for the a-Al_2O_3 layers.
It can be observed that the Eu_2O_3 films show very good transparency in the full spectral range; the absorption coefficient is always well below 0.05 for wavelengths larger than 400 nm. The differences in absorption coefficient between films cannot be considered significant since they are close to our fitting error. The refractive index of the Eu_2O_3 at 620 nm is 2.02 ± 0.02 for Eu00 configuration, very similar to [12], and 2.06 ± 0.02 for Eu11 and Eu01 configurations. This refractive index is much higher than that of Al_2O_3 films, which is 1.76 at 620 nm. This index contrast enables good conditions for the determination of the refractive index of the Eu_2O_3 layers. Therefore, we can consider that the lower value obtained of the Eu_2O_3 in the Eu00 is reliable, and it can be associated to a lower density of the film compared to the films with capping layers.

ii) Chemical characterization.

As-grown Eu-oxide films without capping layer (Eu00 configuration) and with expected nominal stoichiometry Eu_2O_3 were measured as-received and upon low energy (1keV) Ar ion bombardment (procedure employed to remove part of the air contamination present on the surface of the samples). This sputtering process was very useful not only to remove adventitious carbon and adsorbed water but also to increase the signal from the Eu oxide film itself, which was attenuated by them. This is due to the surface sensitivity of the XPS technique and its probing depth limited to a few nanometers thick region. High-resolution XPS data were also recorded for Eu3d and Eu4d core-level peaks in order to determine the oxidation states present in the Eu films. In addition, valence band spectra were also acquired, which are very sensitive to the charge state and provide further insight on the chemical nature of the samples. Detailed XPS line shape analysis revealed no significant differences between the Eu3d, Eu4d and valence band spectra for the samples prior and upon the sputtering cleaning process. As expected, the binding energy values of the Eu photoelectron emission peaks are those reported in the literature for Eu oxide compounds [13,14], together with the O1s counterpart emission, so that the existence of the same oxide phases on the surface and in a deeper region below is clearly confirmed.

Figure 3 shows the XPS spectrum from the 1180 to 1125 eV energy region that corresponds to the Eu 3d photoemission line. After x-ray source satellite removal, Shirley background subtraction and peak deconvolution, XPS spectrum is mainly dominated by the emission of two pronounced peaks

centered at 1134.8 and 1127.2 eV identified as the $3d_{5/2}$ and $3d_{3/2}$ spin-orbit split Eu^{3+} state [15]. There also exists a small contribution shifted at lower binding energy values, respectively, associated to the Eu^{2+} oxidation state. This result is also confirmed by XPS valence band measurements (not shown), which line shape shows a Eu 4f broad emission with multiplet structure in the binding energy region from 5 to 13 eV below the Fermi level together with the O2p level. It corresponds to the $4f^6 \rightarrow 4f^5$ final-state multiplet of trivalent Eu^{3+}. A small contribution of $4f^7 \rightarrow 4f^6$ at a binding energy of 2 eV is also visible, which is characteristic of Eu^{2+} [1,15]. These results allow us to conclude that in the initial amorphous samples (Eu00 configuration), the grown Eu oxide film is mainly composed of Eu_2O_3, with a minor presence of EuO. The origin of this reduced signal is unclear, but it can presumably be a consequence of the ablation process in vacuum.

iii) Structural Properties.

Figures 4 a) and 4 b) show the X-ray diffraction spectra obtained for the three studied configurations after annealing at 500 °C and 850 °C, respectively. The as grown films were found to be amorphous and only showed a broad background (spectra not shown). All the peaks observed in the spectra belong to the Eu_2O_3 films except the peak at $2\theta = 33°$ that correspond to the Si (100) substrate and has been cut off for the analysis [16,17]. No signal from the a-Al_2O_3 is detected in any of the spectra, indicating that the Al_2O_3 layers remain amorphous after the annealing.
Focusing at 500 °C, Fig. 4 a), two peaks for the Eu00 configuration are observed, one at 28.5° and another at 33.15°, almost coincident with the 33° Si peak. These peaks have been associated with the Eu_2O_3 cubic phase. The film with the Eu11 configuration, besides the peaks of the cubic phase, exhibits two additional maxima in the 31-32° region that correspond to the Eu_2O_3 monoclinic phase. Finally, the film with the Eu01 configuration shows only features of the monoclinic phase, that is, some very weak peaks at 29.5° and 30.2° plus the peaks in the 31-32° region. Therefore, the crystalline structure of the films presents a clear dependence on the presence of the buffer and capping layers. In summary, after the annealing at 500 °C, Eu00 film shows only peaks corresponding to the cubic phase, Eu11 exhibits the presence of cubic phase peaks and some features of the monoclinic phase and finally, Eu01 film presents only peaks of the monoclinic phase. It has been reported that in order to obtain a pure Eu_2O_3 monoclinic phase in ceramics, sintering temperatures above 1300 °C are required [6]. Thus, these last results are of great importance since they demonstrate that by depositing a capping layer of Al_2O_3, the formation of the monoclinic phase can be induced at temperatures as low as 500 °C in thin films.
As far as we know, the crystallization temperature of Eu oxide phases in thin films is not fully established and there are few reports in the literature. In some of them, crystallization has been shown to occur at temperatures as low as 600 °C in mesoporous Eu_2O_3 films [18]. However, this temperature might depend on the film deposition method and on the annealing conditions, and it could happen at lower temperatures. The X-rays analysis shows clearly that there are cubic and/or monoclinic phases in our thin sample at 500 °C. However, we cannot rule out co-existence with amorphous phases.

Fig. 4 (b) shows the XRD spectra obtained after the 850 °C annealing. For this temperature, Eu00 still shows the characteristic peaks of the cubic phase. However, some broad features in the region 31°-32°, which can be assigned to the monoclinic phase, start to appear. Eu11 presents the same peaks that appeared after the annealing at 500 °C, but the intensity of the peaks corresponding to the monoclinic phase increases. The most significant change is shown for Eu01 configuration. For this film, it can be observed that in addition to the monoclinic phase peaks, a new peak at 28.5° corresponding to the cubic phase is formed.

In order to obtain an estimation of the evolution of cubic and monoclinic phases in the films, the areas under peaks were integrated. Note that a full quantitative analysis of the films that would require comparison with standards and to take into account the relative intensities of the peaks is beyond the scope of this work. However, the semi-quantitative approach employed allows evaluating relative compositional variations between the different samples. The peak at 33.15° has been carefully deconvoluted from that corresponding to the Si substrate. Once the area of the Si peak has been subtracted, the integrated area under the peaks at 28.5° and 33.15° has been associated to the relative percentage of cubic phase, and the integrated area under all the other peaks has been ascribed to the relative percentage of monoclinic phase. The following expression has been used to estimate the relative percentage of cubic/monoclinic phase:

$$\%\ (cubic/monoclinic)\ phase \approx 100\ \times \frac{area_{cubic/monoclinic}}{area_{cubic}+area_{monoclinic}} \qquad (2)$$

The error in the integrated peak area is 4% and is due to the error limits for the peak identification. The presence of secondary phases, e.g. the amorphous phase, has not been considered. The results are presented in Figure 5. According to the phase diagram that shows the stability of the phases in the rare-earth sesquioxides, the cubic phase is stable at low temperature and low pressures [19,20]. Therefore, the behavior of the Eu_2O_3 films in the Eu01 and Eu11 configurations is in good agreement with this phase diagram because it is found that as the annealing temperature increases the percentage of monoclinic phase increases. At this point, it is also interesting to note that in the as deposited configuration, according to the linear optical properties, the films with the Eu00 configuration had lower density compared to the Eu01 and Eu11 configurations. These as-grown differences could explain why upon annealing at 500 °C the cubic phase is favored for Eu00, whereas Eu11 and Eu01 preferred the monoclinic phase. The presence of compressing and tensile stresses upon the deposition of materials with different composition has been reported for different multilayer systems [21,22]. Moreover, stress-induced stabilization of thermodynamically unfavoured phases in Eu_2O_3 has been recently reported [23]. In that sense, the a-Al_2O_3 capping layer might induce a compressive strain on the Eu_2O_3 layer that could stabilize the denser monoclinic phase upon annealing at 500 °C, although further experiments are required to validate this assumption.

Following, in the Eu01 configuration upon annealing it is found that it exhibits a somewhat unexpected behavior. First, it is found that upon low temperature annealing (500 °C) only the formation of the monoclinic phase is obtained, which is fully in agreement with the previously discussed tensile effect of the a-Al_2O_3 capping layer on the Eu_2O_3 layer. In contrast to the Eu11

configuration, Eu01 does not have a-Al_2O_3 buffer and even so, no cubic phase upon low temperature annealing is detected. However upon annealing at higher temperatures (850 °C) some cubic phase is formed, which is not expected according to the phase diagrams. The reason for the formation of the cubic phase upon further annealing is still unclear. Two scenarios can be proposed. It may be due to the relaxation of the strained monoclinic phase upon annealing, or to the presence of a residual amount of amorphous phase that preferentially crystallizes first in the cubic form. Further studies are needed.

iv) Visible light emission. Photoluminescence (PL).

The as-grown samples showed no measurable emission. Figure 6 shows the normalized photoluminescence spectra obtained for the different configurations after annealing at 500°C (dot lines) and 850 °C (straight lines). A measurement of the Eu_2O_3 bulk target (monoclinic phase) was also performed for comparison and the corresponding spectra is included in the top of the graph. The spectra show the 4f intra-transitions for the Eu^{3+} ions with remarkable differences due to the crystalline phases present in the films. The emissions corresponding to the $^5D_0 \rightarrow {}^7F_0$, $^7F_1$ and $^7F_2$ transitions are identified in the graph. In order to associate the XRD results with the differences between the PL spectra for the different configurations, we will focus on the $^5D_0 \rightarrow {}^7F_2$ transition for the analysis. Besides, $^5D_0 \rightarrow {}^7F_2$ dominates the PL spectra and is very sensitive to the specific crystal field experienced by the ions [24,25].

The PL spectra show a clear evolution from the Eu_2O_3 layer emission in the cubic phase (configuration Eu00), to the pure monoclinic Eu_2O_3 target emission. A splitting of the emission due to the $^5D_0 \rightarrow {}^7F_2$ transition in two peaks becomes evident when the percentage of monoclinic phase increases. For the Eu_2O_3 films with a dominant cubic phase, the emission is characterized by a single peak at 612 nm. Also, for Eu00, the peak at 612 nm is more intense for the spectrum obtained after 500 °C annealing than after the 850 °C annealing. This result agrees with the XRD analysis that shows that there is a relative increase of the monoclinic phase from 500 °C to 850 °C. As a consequence, there is an increase of the peak at 623 nm, due to a small splitting of the $^5D_0 \rightarrow {}^7F_2$ transition in the presence of a weak monoclinic crystal phase (Fig. 5). Remember that according to the equilibrium phase diagram of the rare-earth oxides, the cubic phase of Eu_2O_3 is the stable phase at low temperature [19]. A transformation of the crystalline Eu_2O_3 phase towards the monoclinic structure with the increase of temperature is thus expected.

In the opposite case, the emission of the Eu_2O_3 target (completely monoclinic) [6] presents two main peaks: one at 615 nm and the other, the most intense, at 623 nm. This characteristic transition is therefore attributed to the splitting of $^5D_0 \rightarrow {}^7F_2$ due to the Eu ion embedded in a pure monoclinic phase field and is in agreement with previous works [26–28].

Mixed cases are observed for the emissions at 850 °C of the Eu_2O_3 films in the Eu11 (slightly predominant cubic phase) and Eu01 (slightly dominant monoclinic phase) configurations, agreeing also with the XRD analysis (Fig. 5). Even more, the emission for the Eu_2O_3 in the Eu01 configuration shows very similar features to the Eu_2O_3 target, but the relative intensities between the 615 nm and 623 peaks change. This is due to the fact that the Eu_2O_3 film in Eu01 is not completely crystallized in the monoclinic phase at 850 °C. In the spectrum corresponding to the Eu11 configuration, the peaks are less clearly defined, and the transition $^5D_0 \rightarrow {}^7F_1$ is broader. At this

point, it should be noted that the Eu11 film has a larger amount of a-Al_2O_3 (having both buffer and capping layers). Some mixing might occur at the Eu_2O_3 – a-Al_2O_3 interfaces during deposition due to the high energy of the ions during the PLD process [5,29]. Therefore, part of the emission could be due to Eu^{3+} ions within a-Al_2O_3. Since Al_2O_3 is amorphous, a broader emission peak (more disordered host) of the Eu^{3+} ions is expected for the $^5D_0 \rightarrow {}^7F_J$ transition [30].

These results are relevant for technological applications, since they allow designing thin films with markedly characteristic emissions. The samples with cubic configuration showed a high purity emission (FWHM 5 nm) that could be desirable for applications such as lasers and diodes. However, for some lighting applications, wider emission (FWHM 20 nm) spectra such as that exhibited by the monoclinic phase could be more advantageous.

4. Conclusions

Eu_2O_3 optically active thin films have been fabricated by pulsed laser deposition and post-deposition annealing. Analysis of the structure shows that the initially deposited films are amorphous and they crystallize after annealing at 500 °C, where both cubic and monoclinic Eu_2O_3 crystalline phases are formed. It is demonstrated that the presence of buffer and capping layers of Al_2O_3 influences the relative percentage of these phases in the films. Specifically, it has been found that the deposit of a-Al_2O_3 capping layer favors the formation of the monoclinic phase at low temperatures, when this phase is usually formed at high temperatures (above 1300 °C). This opens an appealing route for tailoring the crystalline structure of Eu_2O_3 at low temperature processing conditions. Moreover, as a consequence, the emission properties of the Eu^{3+} can be tuned since the crystal field effects modify the ion emission characteristics. In particular, the luminescence can be changed from a narrow emission centered at 612 nm to a wider emission centered around 620 nm.

5. Acknowledgments

This work has been financially supported by the Spanish Ministry of Economy and Competitiveness through the projects TEC2012-38901-C02-01, MAT2013-47878-C2-1-R and MAT2013-48009-C4-1-P co-funded with FEDER funds. A.M. acknowledges the financial support through BES-2013-062593. I.C. acknowledges the financial support through JAE-Pre-2011_00578.

6. References

[1] J.N. Beukers, J.E. Kleibeuker, G. Koster, D.H.A. Blank, G. Rijnders, H. Hilgenkamp, et al., Epitaxial EuO thin films by pulsed laser deposition monitored by in situ x-ray photoelectron spectroscopy, Thin Solid Films. 518 (2010) 5173–5176. doi:10.1016/j.tsf.2010.04.071.

[2] G. Bellocchi, G. Franzò, F. Iacona, S. Boninelli, T. Cesca, F. Priolo, et al., Eu^{3+} reduction and efficient light emission in Eu_2O_3 films deposited on Si substrates, Opt. Express. 20 (2012) 5501–5507. http://www.ncbi.nlm.nih.gov/pubmed/22418355.

[3] L. Li, J. Zheng, Y. Zuo, B. Cheng, Q. Wang, Strong Eu^{2+} light emission in Eu silicate through Eu^{3+} reduction in Eu_2O_3/Si multilayer deposited on Si substrates., Nanoscale Res. Lett. 8 (2013) 194. doi:10.1186/1556-276X-8-194.

[4] Y.C. Shin, S.J. Leem, C.M. Kim, S.J. Kim, Y.M. Sung, C.K. Hahn, et al., Deposition of Europium Oxide on Si and its optical properties depending on thermal annealing conditions, J. Electroceramics. 23 (2009) 326–330. doi:10.1007/s10832-008-9449-7.

[5] C.N. Afonso, J. Gonzalo, R. Serna, J. Solis, OPTICAL FILMS MAIN FEATURES OF PULSED LASER, (2000).

[6] A. Quesada, A. del Campo, J.F. Fernández, Sintering behaviour and translucency of dense Eu_2O_3 ceramics, J. Eur. Ceram. Soc. 34 (2014) 1803–1808. doi:10.1016/j.jeurceramsoc.2013.12.034.

[7] R. Serna, M. Jiménez De Castro, J. A. Chaos, A. Suárez-Garcia, C.N. Afonso, M. Fernéndez, et al., Photoluminescence performance of pulsed-laser deposited Al_2O_3 thin films with large erbium concentrations, J. Appl. Phys. 90 (2001) 5120–5125. doi:10.1063/1.1409575.

[8] R. Serna, J.C.G. de Sande, J.M. Ballesteros, C.N. Afonso, Spectroscopic ellipsometry of composite thin films with embedded Bi nanocrystals, J. Appl. Phys. 84 (1998) 4509–4516. doi:10.1063/1.368676.

[9] J. A. Sánchez-García, R. Gago, R. Caillard, A. Redondo-Cubero, J. A. Martin-Gago, F.J. Palomares, et al., Production of nanohole/nanodot patterns on Si(001) by ion beam sputtering with simultaneous metal incorporation., J. Phys. Condens. Matter. 21 (2009) 224009. doi:10.1088/0953-8984/21/22/224009.

[10] F.J. Palomares, E. Paz, F. Soria, J.S. Moya, M. Burianek, M. Muehlberg, et al., Surface Chemistry of Ion Irradiated and Heat-Treated Mullite-Type Bi2Ga4O9 Single Crystals, J. Am. Ceram. Soc. 92 (2009) 2993–2998. doi:10.1111/j.1551-2916.2009.03296.x.

[11] T. Lichtenstein, U. of Rochester. College of Engineering, A. Science, Handbook of Thin Film Materials, College of Engineering and Applied Science, University of Rochester, 1979. https://books.google.es/books?id=ozSaHAAACAAJ.

[12] A. A. Dakhel, Structure, refractive index dispersion and optical absorption properties of evaporated Zn-Eu oxide films, Mater. Chem. Phys. 81 (2003) 56–62. doi:10.1016/S0254-0584(03)00107-X.

[13] D. Briggs, Handbook of X-ray Photoelectron Spectroscopy C. D. Wanger, W. M. Riggs, L. E. Davis, J. F. Moulder and G. E.Muilenberg Perkin-Elmer Corp., Physical Electronics Division,

Eden Prairie, Minnesota, USA, 1979. 190 pp. $195, Surf. Interface Anal. 3 (1981) v–v. doi:10.1002/sia.740030412.

[14] NIST X-ray Photoelectron Spectroscopy (XPS) Database, Version 3.5, (n.d.). http://srdata.nist.gov/xps/ (accessed June 10, 2015).

[15] C. Caspers, M. Müller, A.X. Gray, A.M. Kaiser, A. Gloskovskii, C.S. Fadley, et al., Chemical stability of the magnetic oxide EuO directly on silicon observed by hard x-ray photoemission spectroscopy, Phys. Rev. B. 84 (2011) 205217. http://link.aps.org/doi/10.1103/PhysRevB.84.205217.

[16] F. Saporiti, R.E. Juarez, F. Audebert, M. Boudard, Yttria and ceria doped zirconia thin films grown by pulsed laser deposition, Mater. Res. 16 (2013) 655–660. doi:10.1590/S1516-14392013005000053.

[17] M. A. Niedermeier, D. Magerl, Q. Zhong, A. Nathan, V. Körstgens, J. Perlich, et al., Combining mixed titania morphologies into a complex assembly thin film by iterative block-copolymer-based sol–gel templating, Nanotechnology. 23 (2012) 145602. doi:10.1088/0957-4484/23/14/145602.

[18] Y. Castro, B. Julian, C. Boissiere, B. Viana, H. Amenitsch, D. Grosso, et al., Synthesis, characterization and optical properties of Eu_2O_3 mesoporous thin films, 055705 (2007). doi:10.1088/0957-4484/18/5/055705.

[19] H.R. Hoekstra, Phase Relationships in the Rare Earth Sesquioxides at High Pressure, Inorg. Chem. 5 (1966) 754–757. doi:10.1021/ic50039a013.

[20] G. Chen, N. Stump, R. Haire, J. Peterson, Study of the phase behavior of Eu_2O_3 under pressure via luminescence of Eu3+, J. Alloys Compd. 181 (1992) 503–509. doi:10.1016/0925-8388(92)90347-C.

[21] C.E. Murray, P.R. Besser, C. Witt, J.L. Jordan-Sweet, Stress gradients induced in Cu films by capping layers, Appl. Phys. Lett. 93 (2008) 11–14. doi:10.1063/1.3035853.

[22] J.B. Oliver, P. Kupinski, A. L. Rigatti, A. W. Schmid, J.C. Lambropoulos, S. Papernov, et al., Stress compensation in hafnia/silica optical coatings by inclusion of alumina layers, Opt. Express. 20 (2012) 16596. doi:10.1364/OE.20.016596.

[23] A. Quesada, A. del Campo, J.F. Fernández, Stabilization of cubic phase in dense Eu_2O_3 ceramics, Mater. Lett. 157 (2015) 77–80. doi:10.1016/j.matlet.2015.05.085.

[24] B.M. Walsh, Judd-Ofelt theory: principles and practices, Adv. Spectrocopy Lasers Sens. (2006) 403–433. doi:10.1007/1-4020-4789-4_21.

[25] C.K. Jørgensen, B.R. Judd, Hypersensitive pseudoquadrupole transitions in lanthanides, Mol. Phys. 8 (1964) 281–290. doi:10.1080/00268976400100321.

[26] K.W. Chae, T.R. Park, C. II Cheon, N. In Cho, J. Seog Kim, Luminescence enhancement by the reduction-oxidation synthesis in monoclinic RE_2O_3 (RE=Eu, Gd) phosphors containing Eu^{3+} activator, J. Lumin. 132 (2012) 2293–2301. doi:10.1016/j.jlumin.2012.03.041.

[27] B. Bihari, H. Eilers, B.M. Tissue, Spectra and dynamics of monoclinic Eu_2O_3 and Eu^{3+}:Y_2O_3 nanocrystals, J. Lumin. 75 (1997) 1–10. doi:10.1016/S0022-2313(97)00102-6.

[28] M.O. and M.T. and A.K.A. and N. Matsuda, Luminescence Properties of Rare Earth Ion-Doped Monoclinic Yttrium Sesquioxide, Jpn. J. Appl. Phys. 36 (1997) 6411. http://stacks.iop.org/1347-4065/36/i=10R/a=6411.

[29] J. Schou, Physical aspects of the pulsed laser deposition technique: The stoichiometric transfer of material from target to film, Appl. Surf. Sci. 255 (2009) 5191–5198. doi:10.1016/j.apsusc.2008.10.101.

[30] A. García-Murillo, C. Le Luyer, C. Garapon, C. Dujardin, E. Bernstein, C. Pedrini, et al., Optical properties of europium-doped Gd_2O_3 waveguiding thin films prepared by the sol-gel method, Opt. Mater. (Amst). 19 (2002) 161–168. doi:10.1016/S0925-3467(01)00214-2.

Figure Caption

Figure 1: Schematic representation of the films configuration Eu00, Eu11 and Eu01.

Figure 2: Refractive index (n, straight lines) and extinction coefficient (k, dashed lines) of Eu00, Eu11 and Eu01 as-grown films.

Figure 3: XPS spectrum of Eu3d core level for Eu00 as-grown film.

Figure 4: XRD spectra of Eu00, Eu11 and Eu01 after annealing at 500°C and 850 °C, **a)** and **b)** respectively. Labeled peaks (♦) and (■) correspond to the monoclinic and cubic phases, respectively. The peak at 33° to the Si substrate has been cut off.

Figure 5: Evolution of the monoclinic (top axe) and cubic (bottom axe) phases with the annealing temperature in the Eu00, Eu11 and Eu01 configurations. Data extracted from XRD spectra analysis.

Figure 6: Photoluminescence intensity spectra of Eu00, Eu11, Eu01 and Eu_2O_3 target. $^5D_0 \rightarrow {}^7F_J$ transitions (with J=0, 1, 2) are showed. Dot lines represent the emissions at 500°C, and straight lines at 850°C.

Figure 1

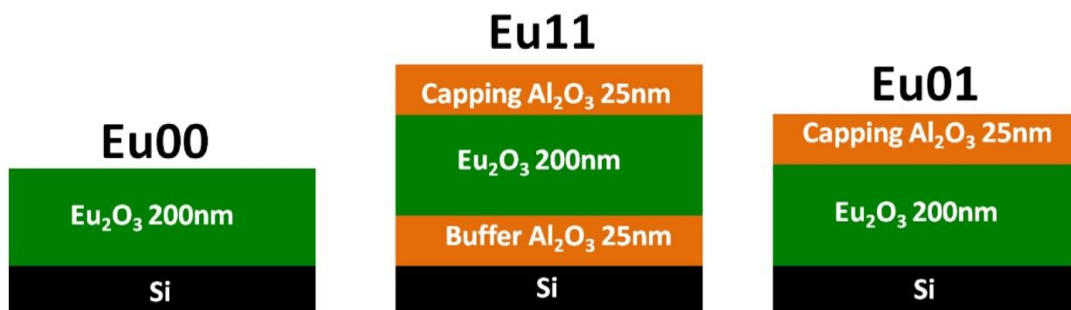

Figure 2

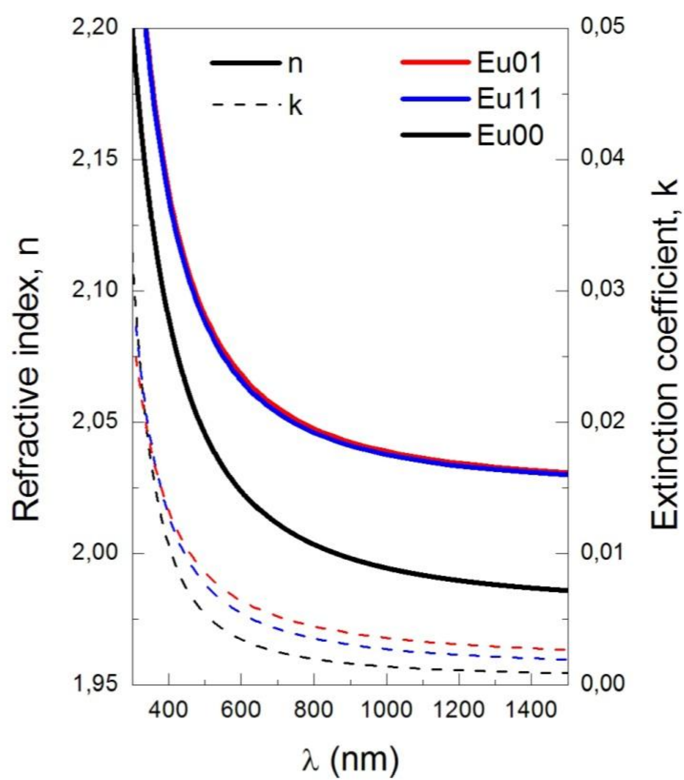

Figure 3

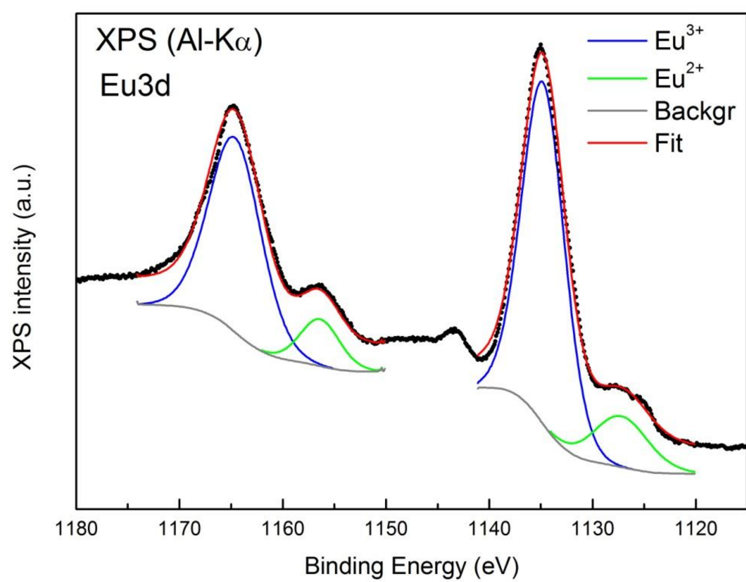

Figure 4

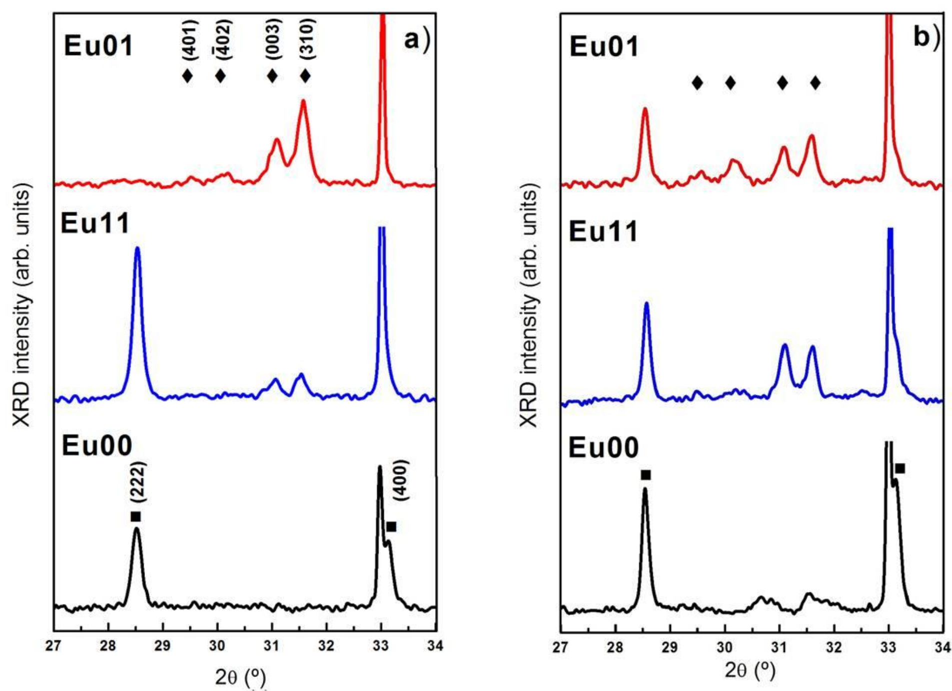

Figure 5

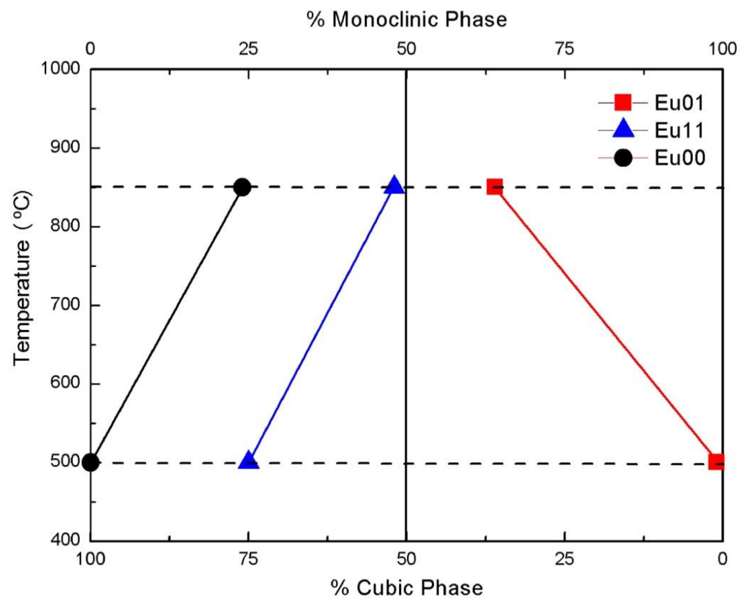

Figure 6